Many-body corrections to cyclotron resonance in monolayer and bilayer graphene

K. Shizuya
Yukawa Institute for Theoretical Physics, Kyoto University, Kyoto 606-8502, Japan
(Received 25 October 2009; published 5 February 2010)

Cyclotron resonance in graphene is studied with focus on many-body corrections to the resonance energies, which evade Kohn's theorem. The genuine many-body corrections turn out to derive from vacuum polarization, specific to graphene, which diverges at short wavelengths. Special emphasis is placed on the need for renormalization, which allows one to determine many-body corrections uniquely from one resonance to another. For bilayer graphene, in particular, both intralayer and interlayer coupling strengths undergo infinite renormalization; as a result, the renormalized velocity and interlayer coupling strength run with the magnetic field. A comparison of theory with the experimental data is made for both monolayer and bilayer graphene.

DOI: 10.1103/PhysRevB.81.075407 PACS number(s): 73.22.Lp, 73.43.Lp, 76.40.+b

I. INTRODUCTION

Graphene, a monolayer graphite, attracts great attention for its unusual electronic transport[1–6] as well as its potential applications. It supports as charge carriers massless Dirac fermions, which lead to such exotic phenomena as the half-integer quantum-Hall (QH) effect and minimal conductivity.

The multispinor character of the electrons in graphene derives from the sublattice structure of the underlying honeycomb lattice, and this immediately implies, in the low-energy effective theory of graphene, the quantum nature of the vacuum state;[7] the conduction and valence bands are related by charge conjugation and, in particular, the latter acts as the Dirac sea. Graphene in a magnetic field B thus gives rise to a particle-hole symmetric "relativistic" pattern of Landau levels, with spectra $\epsilon_n \propto \pm\sqrt{|n|}\sqrt{B}$ unequally spaced, together with four characteristic zero-energy Landau levels (whose presence has a topological origin[8]).

This nontrivial vacuum structure is the key feature that distinguishes graphene and its multilayers from conventional QH systems. In particular, bilayer graphene[9] supports, as a result of interlayer coupling, massive fermions, which, in a magnetic field, again develop a particle-hole symmetric tower of Landau levels, with an octet of zero-energy levels.[10] Bilayer graphene has a unique property that its band gap is externally controllable.[11–14]

Graphene and its multilayers give rise to rich spectra of cyclotron resonance, with resonance energies varying from one transition to another within the electron band or the hole band, and, notably, even between the two bands. This is in sharp contrast with conventional QH systems with a parabolic dispersion, where cyclotron resonance (optically induced at zero-momentum transfer $\mathbf{k}=0$) takes place between adjacent Landau levels, hence at a single frequency $\omega_c = eB/m^*$ which, according to Kohn's theorem,[15] is unaffected by Coulomb interactions. Nonparabolicity[16] of the electronic spectra in graphene evades Kohn's theorem and offers the possibility to detect the many-body corrections to cyclotron resonance, as discussed theoretically for monolayer graphene.[17,18]

Experiment has already studied via infrared spectroscopy cyclotron resonance in monolayer[19,20] and bilayer[21] graphene, and verified the characteristic features of the associated Landau levels. Data generally show no clear sign of the many-body effect, except for one[19] on monolayer graphene.

The purpose of this paper is to study the many-body effect on cyclotron resonance in graphene, by constructing an effective theory of cyclotron resonance within the single-mode approximation. It is shown that the genuine many-body corrections arise from vacuum polarization, specific to graphene, which actually diverges logarithmically at short wavelengths and requires renormalization. Our approach in part recovers results of earlier studies[17,18] on monolayer graphene but essentially differs from them in this handling of cutoff-dependent corrections by renormalization, which allows one to determine many-body corrections uniquely from one resonance to another. Our analysis also reveals that for bilayer graphene both intralayer and interlayer coupling strengths undergo renormalization.[22,23] We compare theory with the experimental data for monolayer and bilayer graphene.

In Sec. II we briefly review the effective theory of graphene and, in Sec. III, study cyclotron resonance in monolayer graphene, with focus on the many-body corrections and renormalization. In Sec. IV we extend our analysis to bilayer graphene. Section V is devoted to the summary and discussion.

II. MONOLAYER GRAPHENE

Graphene has a honeycomb lattice which consists of two triangle sublattices of carbon atoms. The electrons in graphene are described by a two-component spinor field (ψ_A, ψ_B) on two inequivalent lattice sites (A,B). The electrons acquire a linear spectrum near the two inequivalent Fermi points (K and K') in the Brillouin zone, with the "light velocity" $v_0 = (\sqrt{3}/2)a_L\gamma_0/\hbar \approx 10^6$ m/s related to the intralayer coupling $\gamma_0 \equiv \gamma_{AB} \approx 2.9$ eV (with $a_L = 0.246$ nm).

Their low-energy features are described by an effective Hamiltonian of the form[7]

$$H_0 = \int d^2\mathbf{x}[\psi^\dagger \mathcal{H}_+ \psi + \psi'^\dagger \mathcal{H}_- \psi'],$$

$$\mathcal{H}_\pm = v_0(\sigma_1\Pi_1 + \sigma_2\Pi_2 \mp \delta m\sigma_3) - eA_0, \qquad (2.1)$$

where $\Pi_i = -i\partial_i + eA_i$ [$i=(1,2)$ or (x,y)] involve coupling to external electromagnetic potentials $A_\mu = (A_i, A_0)$. Here

$\psi \equiv (\psi_1, \psi_2)^t = (\psi_A, \psi_B)^t$ stands for the electron field at one (or K) valley, and $\psi' = (\psi'_B, \psi'_A)^t$ to one at another valley, with A and B referring to the associated lattice sites. δm denotes a possible tiny asymmetry in sublattices.

Let us place graphene in a uniform magnetic field $B_\perp = B > 0$; we set $A_i \to B(-y, 0)$. The electron spectrum then forms an infinite tower of Landau levels L_n of energy

$$\epsilon_n = s_n \omega_c \sqrt{|n| + (\delta m)^2 \ell^2/2} \tag{2.2}$$

labeled by integers $n = 0, \pm 1, \pm 2, \ldots$, and p_x (or $y_0 \equiv \ell^2 p_x$ with the magnetic length $\ell \equiv 1/\sqrt{eB}$). Here $s_n \equiv \mathrm{sgn}\{n\} = \pm 1$ specifies the sign of the energy ϵ_n and

$$\omega_c \equiv \sqrt{2} v_0/\ell \approx 36.3 \times v_0[10^6 \text{ m/s}] \sqrt{B[\mathrm{T}]} \text{ meV} \tag{2.3}$$

is the basic cyclotron frequency; $v_0[10^6 \text{ m/s}]$ stands for v_0 in units of 10^6 m/s and $B[\mathrm{T}]$ stands for a magnetic field in tesla.

Suppose, without loss of generality, that $\delta m > 0$. Then the $n=0$ level at the K valley has positive energy $\epsilon_{0_+} = v_0 \delta m > 0$ while the $n=0$ level at the K' valley has negative energy $\epsilon_{0_-} = -v_0 \delta m$. In general, the spectra at the two valleys are related as $\epsilon_n|_K = -\epsilon_{-n}|_{K'}$. With the electron spin taken into account (and Zeeman splitting ignored for simplicity), each Landau level is thus fourfold degenerate, except for the doubly degenerate $n = 0_\pm$ levels split in valley. With this feature in mind, we shall set the asymmetry $\delta m \to 0$ in what follows.

The Coulomb interaction is written as

$$H^{\mathrm{Coul}} = \frac{1}{2} \sum_{\mathbf{p}} v_{\mathbf{p}} :\rho_{-\mathbf{p}} \rho_{\mathbf{p}}:, \tag{2.4}$$

where $\rho_{\mathbf{p}}$ is the Fourier transform of the electron density $\rho = \psi^\dagger \psi + \psi'^\dagger \psi'$ (here $\psi^\dagger \psi$, e.g., is summed over spinor and spin indices); $v_{\mathbf{p}} = 2\pi\alpha/(\epsilon_{\mathrm{b}}|\mathbf{p}|)$ is the Coulomb potential with the fine-structure constant $\alpha = e^2/(4\pi\epsilon_0) \approx 1/137$ and the substrate dielectric constant ϵ_{b}.

The Landau-level structure is made explicit by passing to the $|n, y_0\rangle$ basis, with the expansion $\psi(\mathbf{x}, t) = \Sigma_{n,y_0} \langle \mathbf{x}|n, y_0\rangle \psi_n(y_0, t)$. (For conciseness, we shall only display the ψ sector from now on.) The Hamiltonian H_0 is thereby rewritten as

$$H_0 = \int dy_0 \sum_{n=-\infty}^{\infty} \psi_n^\dagger(y_0, t) \epsilon_n \psi_n(y_0, t) \tag{2.5}$$

and the charge density $\rho_{-\mathbf{p}}(t) = \int d^2\mathbf{x} e^{i\mathbf{p}\cdot\mathbf{x}} \psi^\dagger \psi$ as[24]

$$\rho_{-\mathbf{p}} = \sum_{k,n=-\infty}^{\infty} \rho^{kn}_{-\mathbf{p}} = \sum_{k,n=-\infty}^{\infty} g^{kn}_{\mathbf{p}} R^{kn}_{\mathbf{p}},$$

$$R^{kn}_{\mathbf{p}} = \gamma_{\mathbf{p}} \int dy_0 \psi_k^\dagger(y_0, t) e^{i\mathbf{p}\cdot\mathbf{r}} \psi_n(y_0, t), \tag{2.6}$$

where $\gamma_{\mathbf{p}} = e^{-\ell^2 \mathbf{p}^2/4}$; and $\mathbf{r} = (r_x, r_y) = (i\ell^2 \partial/\partial y_0, y_0)$ stands for the center coordinate with uncertainty $[r_x, r_y] = i\ell^2$. The charge operators $R^{kn}_{\mathbf{p}}$ obey the W_∞ algebra[25]

$$[R^{mm'}_{\mathbf{k}}, R^{nn'}_{\mathbf{p}}] = \delta^{n'n} e^{k^\dagger p/2} R^{mn'}_{\mathbf{k}+\mathbf{p}} - \delta^{n'm} e^{p^\dagger k/2} R^{nm'}_{\mathbf{k}+\mathbf{p}}, \tag{2.7}$$

where $k^\dagger p = \mathbf{k}\cdot\mathbf{p} - i\mathbf{k}\times\mathbf{p}$ with $\mathbf{k}\times\mathbf{p} \equiv k_x p_y - k_y p_x$. This actually consists of two W_∞ algebras associated with intralevel center-motion[25] and interlevel mixing[26] of electrons.

The coefficient matrix $g^{kn}_{\mathbf{p}}$ is given by

$$g^{kn}_{\mathbf{p}} = \frac{1}{2} b_k b_n (f^{|k|-1,|n|-1}_{\mathbf{p}} + s_k s_n f^{|k|,|n|}_{\mathbf{p}}), \tag{2.8}$$

where $b_n = 1$ for $n \neq 0$ and $b_0 = \sqrt{2}$:

$$f^{kn}_{\mathbf{p}} = \sqrt{\frac{n!}{k!}} \left(\frac{-\ell p}{\sqrt{2}}\right)^{k-n} L_n^{(k-n)}\left(\frac{1}{2}\ell^2 \mathbf{p}^2\right) \tag{2.9}$$

for $k \geq n \geq 0$ and $f^{nk}_{\mathbf{p}} = (f^{kn}_{-\mathbf{p}})^\dagger$; $p = p_x - i p_y$. Note that $g^{kn}_{\mathbf{p}}$ are essentially the same at the two valleys, i.e., $g^{kn}_{\mathbf{p}}|_{K'} = g^{kn}_{\mathbf{p}}|_K$ and $g^{k0_-}_{\mathbf{p}}|_{K'} = g^{k0_+}_{\mathbf{p}}|_K$ for $|k| \geq 1$ and $|n| \geq 1$; one simply needs to specify $n = 0_\pm$ accordingly.

III. CYCLOTRON RESONANCE

In this section we study cyclotron resonance in monolayer graphene. Let us first note that the charge operator $\rho^{kn}_{-\mathbf{p}} = g^{kn}_{\mathbf{p}} R^{kn}_{\mathbf{p}}$ in Eq. (2.6) annihilates an electron at the nth level L_n and creates one at the kth level L_k. One may thus associate it with the interlevel transition $L_n \to L_k$ or regard it as an interpolating operator for the exciton consisting of a hole at L_n and an electron at L_k.

To describe such inter-Landau-level excitations one can make use of a nonlinear realization of the W_∞ algebra, as is familiar from the theory of quantum-Hall ferromagnet.[27] One may start with a given ground state $|G\rangle$ and describe an excited collective state $|\tilde{G}\rangle$ over it as a local rotation in (n, y_0) space

$$|\tilde{G}\rangle = e^{-i\mathcal{O}}|G\rangle, \tag{3.1}$$

where the operator $e^{-i\mathcal{O}}$ with

$$\mathcal{O} = \sum_{\mathbf{p}} \gamma_{\mathbf{p}}^{-1} \Phi^{kn}_{\mathbf{p}} R^{kn}_{\mathbf{p}} \tag{3.2}$$

locally rotates $|G\rangle$ by "angles" $\Phi^{kn}_{\mathbf{p}}$, which define textures in (n, y_0) space. (Remember here that $\rho_{\mathbf{p}} \sim R^{kn}_{\mathbf{p}}$ are diagonal in spin so that $\Phi^{kn}_{\mathbf{p}}$ carry the spin index as well, though it is suppressed. In principle, one has to retain in $\mathcal{O}$ all possible pairs $\Phi^{kn}_{\mathbf{p}}$ and $(\Phi^{kn}_{\mathbf{p}})^\dagger = \Phi^{nk}_{-\mathbf{p}}$ contributing to the $L_n \to L_k$ transition.)

Repeated use of the charge algebra in Eq. (2.7) allows one to express the texture-state energy $\langle\tilde{G}|H|\tilde{G}\rangle = \langle G|e^{i\mathcal{O}} H e^{-i\mathcal{O}}|G\rangle$ with $H = H_0 + H^{\mathrm{Coul}}$ as a functional of $\Phi^{kn}_{\mathbf{p}}$ or its $\mathbf{x}$-space representative $\Phi^{kn}(\mathbf{x}, t)$. The kinetic term for Φ^{kn} is supplied from the electron kinetic term and one can write the effective Lagrangian for Φ as

$$L_\Phi = \langle\tilde{G}|(i\partial_t - H)|\tilde{G}\rangle = \langle G|e^{i\mathcal{O}}(i\partial_t - H)e^{-i\mathcal{O}}|G\rangle. \tag{3.3}$$

This representation systematizes the single-mode approximation[25] (SMA) within a variational framework.[26] The present theory thus embodies the nonperturbative features of the SMA.

Indeed, for a transition from the filled level L_n (with density $\bar{\rho}_n$) to the empty level L_k, one finds

$$L_\Phi = \bar{\rho}_n \sum_{\mathbf{p}} \Phi^{nk}_{-\mathbf{p}}(i\partial_t - \epsilon^{\rm exc}_{\mathbf{p}})\Phi^{kn}_{\mathbf{p}} + \cdots \tag{3.4}$$

with the excitation spectrum given by the SMA formula

$$\epsilon^{\rm exc}_{\mathbf{p}} = \langle G|[\rho^{nk}_{\mathbf{p}},[H,\rho^{kn}_{-\mathbf{p}}]]|G\rangle/\langle G|\rho^{nk}_{\mathbf{p}}\rho^{kn}_{-\mathbf{p}}|G\rangle, \tag{3.5}$$

i.e., as the oscillator strength divided by the static structure factor

$$\langle G|\rho^{nk}_{\mathbf{p}}\rho^{kn}_{-\mathbf{p}}|G\rangle/\Omega = \bar{\rho}_n \gamma^2_{\mathbf{p}}|g^{kn}_{\mathbf{p}}|^2, \tag{3.6}$$

where $\Omega = \int d^2\mathbf{x}$.

Let us first consider the $n=0_\pm \to n=1$ transitions at filling factor $\nu=2$ with all $n\le 0_\pm$ levels filled and all $n\ge 1$ levels empty. A laborious direct calculation of Eq. (3.5) yields $\epsilon^{\rm exc}_{\mathbf{k}} = \epsilon_1 - \epsilon_0 + \Delta\epsilon^{10}_{\mathbf{k}}$ with

$$\Delta\epsilon^{10}_{\mathbf{k}} = \bar{\rho}_0 v_{\mathbf{k}} \gamma^2_{\mathbf{k}} |g^{10}_{\mathbf{k}}/g^{00}_{\mathbf{k}}|^2 + \sum_{\mathbf{p}} v_{\mathbf{p}} \gamma^2_{\mathbf{p}} I_{\mathbf{p},\mathbf{k}},$$

$$I_{\mathbf{p},\mathbf{k}} = \sum_{n\le 0} (|g^{0n}_{\mathbf{p}}|^2 - |g^{1n}_{-\mathbf{p}}|^2) - c_{\mathbf{p},\mathbf{k}} g^{11}_{\mathbf{p}} g^{00}_{-\mathbf{p}}, \tag{3.7}$$

where $\gamma^2_{\mathbf{k}} = e^{-\ell^2\mathbf{k}^2/2}$ and $c_{\mathbf{p},\mathbf{k}} = \cos(\ell^2 \mathbf{p}\times\mathbf{k})$.

When the $n=0_\pm$ level is partially filled, $\Delta\epsilon^{10}_{\mathbf{k}}$ involves the following contribution:

$$\delta\epsilon^{10}_{\mathbf{k}} = \sum_{\mathbf{p}} v_{\mathbf{p}} \gamma^2_{\mathbf{p}} [|g^{01}_{\mathbf{p}}/g^{00}_{\mathbf{p}}|^2 \bar{s}(\mathbf{p}+\mathbf{k})/\gamma^2_{\mathbf{p}+\mathbf{k}} + (c_{\mathbf{p},\mathbf{k}} g^{11}_{\mathbf{p}}/g^{00}_{\mathbf{p}} - 1)\bar{s}(\mathbf{p})/\gamma^2_{\mathbf{p}}], \tag{3.8}$$

where $\bar{s}(\mathbf{p})$ stands for the projected static-structure factor defined as $\langle G|\rho^{00}_{-\mathbf{p}}\rho^{00}_{\mathbf{p}}|G\rangle/\Omega = \bar{\rho}_0\{\bar{\rho}_0\delta_{\mathbf{p},0} + \bar{s}(\mathbf{p})\}$. The determination of $\bar{s}(\mathbf{p})$ is a highly nontrivial task which requires an exact diagonalization study of model systems[16] and is not attempted here. We instead focus on the case of integer filling, for which $\bar{s}(\mathbf{p})$ is taken to vanish.

Equation (3.7), together with Eq. (3.8), essentially agrees with the result of MacDonald and Zhang[28] for the $L_0 \to L_1$ transition in the standard QH system. The key difference is that quantum fluctuations in $I_{\mathbf{p},\mathbf{k}}$ now involve a sum $\Sigma_{n\le -1}(\cdots)$ over infinitely many Landau levels in the valence band (or the Dirac sea). Actually, one can verify that the SMA expressions (3.7) and (3.8) equally apply to a general interlevel transition $L_a \to L_b$ if one sets the superscripts $0\to a$ and $1\to b$, in an obvious fashion, and takes the sum Σ_n over filled levels.

To be precise, the $0\to 1$ transition of our interest consists of four channels, $(0_+ \to 1)|_K$ and $(0_- \to 1)|_{K'}$ each with spin $s_z = \pm 1/2$. One therefore has to consider mixing of four Φ^{10} to determine $\epsilon^{\rm exc}_{\mathbf{k}}$. Actually only the first term $\propto v_{\mathbf{k}}|g^{10}_{\mathbf{k}}|^2$ in Eq. (3.7), which comes from the direct Coulomb exchange, is responsible for such mixing[17,18] because the rest of terms are diagonal in spin and valley. Such direct terms $\propto v_{\mathbf{k}}|g^{ba}_{-\mathbf{k}}|^2$ (with $b\ne a$) in general vanish for $\mathbf{k}\to 0$ and mixing thus takes place only for $\mathbf{k}\ne 0$. In what follows we focus on the $\mathbf{k}=0$ excitation energies $\epsilon^{\rm exc}_{\mathbf{k}=0}$ with no mixing taken into account. In addition, we make no distinction between the $0_\pm$ levels because $g^{kn}_{\mathbf{p}}$ are essentially the same at the two valleys, as noted in Sec. II.

The cyclotron-resonance energy for a general $L_a \to L_b$ transition with the Landau levels filled up to $n=n_{\rm f}$ is written as $\epsilon^{\rm exc}_{\mathbf{k}=0} = \epsilon_b - \epsilon_a + \Delta\epsilon^{b\leftarrow a}_{\mathbf{k}=0}$ with

$$\Delta\epsilon^{b\leftarrow a}_{\mathbf{k}=0} = \sum_{\mathbf{p}} v_{\mathbf{p}}\gamma^2_{\mathbf{p}} \Big[\sum_{n\le n_{\rm f}} (|g^{an}_{-\mathbf{p}}|^2 - |g^{bn}_{-\mathbf{p}}|^2) - g^{bb}_{\mathbf{p}} g^{aa}_{-\mathbf{p}} \Big]. \tag{3.9}$$

This is the basic formula we use in what follows. Note that $n_{\rm f} = 1, 0_+, -1, -2, -3, \ldots$ correspond to the filling factors $\nu = 4n_{\rm f}+2 = 6, 2, -2, -6, -10, \ldots$, respectively. The $\Sigma_{n\le n_{\rm f}}(|g^{an}_{\mathbf{p}}|^2 - |g^{bn}_{-\mathbf{p}}|^2)$ term refers to the change in quantum fluctuations, via the $a\to b$ transition, of the filled states. Its structure is easy to interpret physically: as an electron is excited from L_a to L_b, $|n=a, y_0\rangle \to |n=b, y_0'\rangle$, virtual transitions from any filled levels to the $|b, y_0'\rangle$ state are forbidden while those to the newly unoccupied $|a, y_0\rangle$ state are allowed to start.

For standard QH systems this correction $\Delta\epsilon^{b\leftarrow a}_{\mathbf{k}=0}$ vanishes for each transition to the adjacent level, $L_n \to L_{n+1}$, according to Kohn's theorem.[15] Indeed, one can verify, for the $0\to 1$ transition, the relation

$$|g^{00}_{-\mathbf{p}}|^2 - |g^{10}_{\mathbf{p}}|^2 - g^{11}_{\mathbf{p}} g^{00}_{-\mathbf{p}} = 0 \tag{3.10}$$

(with $g^{00}_{\mathbf{p}} \to 1$ and $g^{10}_{\mathbf{p}} \to -\ell p/\sqrt{2}$) and analogous ones for other $L_n \to L_{n+1}$ as well.

Interestingly, it happens that Eq. (3.10) also holds for the $0_\pm \to 1$ transition in graphene, with $g^{00}_{\mathbf{p}}=1$, $g^{10}_{\mathbf{p}} = -\ell p/2$, and $g^{11}_{\mathbf{p}} = 1 - \ell^2\mathbf{p}^2/4$. Any nonzero shift $\Delta\epsilon^{1\leftarrow 0}_{\mathbf{k}=0}$ for the $0\to 1$ cyclotron resonance therefore comes from the quantum fluctuations of the Dirac sea and actually diverges logarithmically with the number $N_{\rm L}$ of filled Landau levels in the sea

$$\Delta\epsilon^{1\leftarrow 0}_{\mathbf{0}} = \sum_{\mathbf{p}} v_{\mathbf{p}}\gamma^2_{\mathbf{p}} \sum_{-N_{\rm L}\le n\le -1} (|g^{0n}_{-\mathbf{p}}|^2 - |g^{1n}_{\mathbf{p}}|^2) = V_c \mathcal{C}_N,$$

$$\mathcal{C}_N \approx (\sqrt{2}/8)(\log N_{\rm L} - 1.017), \tag{3.11}$$

where

$$V_c \equiv \alpha/(\epsilon_b \ell) \approx (56.1/\epsilon_b)\sqrt{B[{\rm T}]}\ {\rm meV}. \tag{3.12}$$

$\mathcal{C}_N$ agrees[29] with the result of earlier works[17,18] obtained by a different method.

This divergence in $\mathcal{C}_N$ derives from short-wavelength vacuum polarization and is present even for $B=0$. To see this one may evaluate the Coulomb exchange correction in free space (with $\alpha \to \alpha/\epsilon_b$), using the instantaneous photon and fermion propagators $v_{\mathbf{k}} = 2\pi\alpha/(\epsilon_b|\mathbf{k}|)$ and $iS(\mathbf{p}) = \sigma_i p_i/(2|\mathbf{p}|)$:

$$\sum_{\mathbf{k}} v_{\mathbf{k}} iS(\mathbf{p}+\mathbf{k}) = \sigma\cdot\mathbf{p}\frac{\alpha}{8\epsilon_b}\log(C\Lambda^2/\mathbf{p}^2) \tag{3.13}$$

with momentum cutoff $|\mathbf{k}|\le\Lambda$ and some constant C.

This divergent correction causes infinite renormalization[30] of velocity v_0 in the electron kinetic term $\propto v_0\sigma^i\partial_i$; Eq. (3.13) agrees with an earlier result of Ref. 30. It vanishes at $\mathbf{p}=0$ but, for $B\ne 0$, turns into a nonvanishing energy gap, with $\mathbf{p}^2 \to 2eB = 2/\ell^2$. Actually, this diverging piece precisely agrees with that in Eq. (3.11), if one simply chooses the

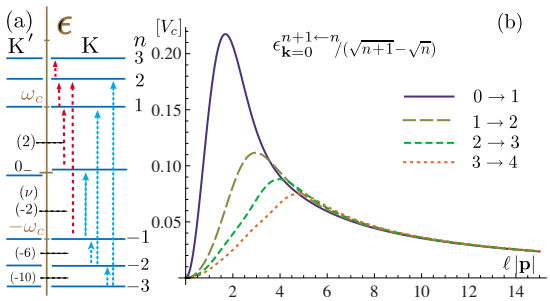

FIG. 1. (Color online) (a) Cyclotron resonance; circularly polarized light can distinguish between two classes of transitions indicated by different types of arrows. (b) Momentum profiles of the many-body corrections $\Delta\epsilon_{\mathbf{k}=0}^{n+1\leftarrow n}/(\sqrt{n+1}-\sqrt{n})$ in units of V_c for $n=0$, 1, 2, and 3.

"Fermi momentum" Λ so that the Dirac sea accommodates the same number of electrons as in the $B\neq 0$ case, $N_{\rm sea}=\Lambda^2/4\pi\approx N_L/2\pi\ell^2$, i.e., $\Lambda^2\approx 2N_{\rm L}/\ell^2$.

Since such an infinite correction is already present for $B=0$, it does not make sense to discuss the magnitude of the cutoff-dependent number $\mathcal{C}_N$ in Eq. (3.11). The legitimate procedure is to renormalize v_0 by rescaling

$$v_0 = Z_v v_0^{\rm ren} \tag{3.14}$$

and put reference to the cutoff into Z_v with $v_0^{\rm ren}$ regarded as an observable quantity.

The renormalized velocity $v_0^{\rm ren}$ is defined by referring to a specific resonance. Let us take the $0\to 1$ resonance and choose to absorb the entire $O(V_c)$ correction at some reference scale (e.g., at magnetic field B_0) into Z_v, i.e., we write

$$\epsilon_{\mathbf{k}=0}^{1\leftarrow 0}\overset{\nu=2}{=}\epsilon_1+\Delta\epsilon_{\mathbf{k}=0}^{1\leftarrow 0}=\sqrt{2}v_0^{\rm ren}|_B/\ell\equiv\omega_c^{\rm ren}|_B \tag{3.15}$$

by setting

$$Z_v=1-\frac{\alpha}{\sqrt{2}v_0\epsilon_b}\mathcal{C}_N=1-\frac{\alpha}{8v_0\epsilon_b}\log\frac{\Lambda^2}{\kappa^2}, \tag{3.16}$$

where $\kappa^2=(\text{const.})eB_0$. The renormalized velocity then depends on B or runs with B

$$v_0^{\rm ren}|_B=v_0^{\rm ren}|_{B_0}-\frac{\alpha}{8\epsilon_b}\log(B/B_0), \tag{3.17}$$

decreasing slightly for $B>B_0$; actually the correction is rather small (about 3% for $B/B_0\sim 2$ and $\epsilon_b\sim 5$ with $v_0^{\rm ren}\sim c/300$). With such B dependence in mind, we denote $v_0^{\rm ren}|_B$ as $v_0^{\rm ren}$ and $\omega_c^{\rm ren}|_B$ as $\omega_c^{\rm ren}$ from now on.

The divergences in $\epsilon_{\mathbf{k}}^{\rm exc}=\epsilon_k-\epsilon_n+\Delta\epsilon_{\mathbf{k}}$ for all other resonances, as illustrated in Fig. 1(a), are taken care of by this velocity renormalization. The finite corrections $\propto V_c$ after renormalization then make sense as genuine observable corrections. In particular, for several intraband channels $L_n\to L_{n+1}$ at filling factor $\nu=4n_{\rm f}+2$, direct calculations yield

$$\epsilon_{\mathbf{k}=0}^{2\leftarrow 1}\overset{\nu=6}{=}(\sqrt{2}-1)\{\omega_c^{\rm ren}-0.264V_c\},$$

$$\epsilon_{\mathbf{k}=0}^{3\leftarrow 2}\overset{\nu=10}{=}(\sqrt{3}-\sqrt{2})\{\omega_c^{\rm ren}-0.358V_c\},$$

$$\epsilon_{\mathbf{k}=0}^{4\leftarrow 3}\overset{\nu=14}{=}(\sqrt{4}-\sqrt{3})\{\omega_c^{\rm ren}-0.419V_c\},$$

$$\epsilon_{\mathbf{k}=0}^{5\leftarrow 4}\overset{\nu=18}{=}(\sqrt{5}-\sqrt{4})\{\omega_c^{\rm ren}-0.464V_c\}, \tag{3.18}$$

where $V_c=\alpha/(\epsilon_b\ell)$. The Coulomb corrections, shown numerically here, are analytically calculable. The excitation spectra $\epsilon_{\mathbf{k}}$ in the hole band are essentially the same

$$\epsilon_{\mathbf{k}}^{-n\leftarrow-(n+1)}|_{n_{\rm f}=-(n+1)}^{\nu=-(4n+2)}=\epsilon_{\mathbf{k}}^{n+1\leftarrow n}|_{n_{\rm f}=n}^{\nu=4n+2} \tag{3.19}$$

reflecting the particle-hole symmetry.

Figure 1(b) shows some of the momentum profiles $\gamma_{\mathbf{p}}^2[\cdots]$ in $\Delta\epsilon_{\mathbf{k}=0}^{n+1\leftarrow n}$ of Eq. (3.9), which, when integrated over $\ell|\mathbf{p}|$, give $\Delta\epsilon_{\mathbf{k}=0}^{n+1\leftarrow n}/(\sqrt{n+1}-\sqrt{n})$ in units of V_c. It is clearly seen that the slowly decreasing high-momentum tails $\sim(\sqrt{2}/4)/(\ell|\mathbf{p}|)$ are responsible for the ultraviolet (UV) divergence and that the finite observable corrections $\propto V_c$ are uniquely determined from the profiles in the low-momentum region $\ell|\mathbf{p}|\lesssim 15$.

A look into the structure of the total current operator tells us that the optically induced cyclotron resonance (for $\mathbf{k}=0$) in graphene is governed by the selection rule $\Delta|n|=\pm 1$, in contrast to the "nonrelativistic" rule $\Delta n=\pm 1$. In particular, there are two classes of transitions (i) $-n\to\pm(n-1)$ and (ii) $\pm(n-1)\to n$ (with $n\geq 1$), which are distinguished[31] by use of circularly polarized light ($\propto A_x\pm iA_y$); see Appendix B

As a result, graphene supports interband cyclotron resonances. The lowest channels are open at $\nu=-2$ with

$$\epsilon_{\mathbf{k}=0}^{2\leftarrow -1}\overset{\nu=-2}{=}(\sqrt{2}+1)\{\omega_c^{\rm ren}+0.122V_c\},$$

$$\epsilon_{\mathbf{k}=0}^{1\leftarrow -2}\overset{\nu=-2}{=}(\sqrt{2}+1)\{\omega_c^{\rm ren}+0.155V_c\}. \tag{3.20}$$

Some other interband channels yield

$$\epsilon_{\mathbf{k}=0}^{1\leftarrow -2}\overset{\nu=-6}{=}(\sqrt{2}+1)\{\omega_c^{\rm ren}+0.084V_c\},$$

$$\epsilon_{\mathbf{k}=0}^{3\leftarrow -2}\overset{\nu=-6}{=}(\sqrt{2}+\sqrt{3})\{\omega_c^{\rm ren}+0.058V_c\},$$

$$\epsilon_{\mathbf{k}=0}^{2\leftarrow -3}\overset{\nu=-6}{=}(\sqrt{2}+\sqrt{3})\{\omega_c^{\rm ren}+0.114V_c\},$$

$$\epsilon_{\mathbf{k}=0}^{2\leftarrow -3}\overset{\nu=-10}{=}(\sqrt{2}+\sqrt{3})\{\omega_c^{\rm ren}+0.044V_c\}. \tag{3.21}$$

It is now clear that cyclotron resonance is best analyzed by plotting the rescaled energies $\epsilon_{\mathbf{k}=0}^{b\leftarrow a}/|s_b\sqrt{|b|}-s_a\sqrt{|a|}|$ as a function of $\sqrt{B}$ or B. The Coulombic many-body effect will be seen as a variation in the characteristic velocity $v_0^{\rm ren}[1+O(V_c)]$ from one resonance to another and a deviation of $\omega_c^{\rm ren}$ from the $\sqrt{B}$ behavior would indicate the running of $v_0^{\rm ren}$ with B.

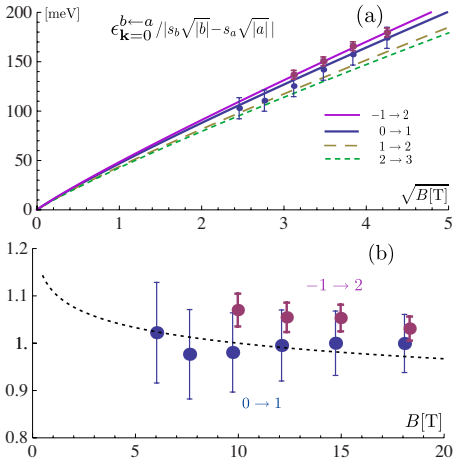

FIG. 2. (Color online) (a) Rescaled cyclotron-resonance energies as a function of $\sqrt{B}$ with $v_0^{\rm ren} \approx 1.13 \times 10^6$ m/s (at $B=10$ T) and $V_c \approx 12\sqrt{B[\mathrm{T}]}$ meV ($\epsilon_b \sim 5$). The experimental data on $\epsilon_{\mathbf{k}=0}^{1\leftarrow 0}$ and $\epsilon_{\mathbf{k}=0}^{2\leftarrow -1}/(\sqrt{2}+1)$ are quoted from Ref. 19 with error bars inferred from the symbol size in the original data. (b) The same data plotted in units of $\omega_c = \sqrt{2}v_0/\ell$ (with $v_0 \to v_0^{\rm ren}|_{B=10\ \mathrm{T}}$) as a function of B. The dotted curve represents a possible profile of the running of $v_0^{\rm ren}|_B$, normalized to 1 at $B=10$ T, with $v_0^{\rm ren}|_{B=10\ \mathrm{T}} \approx 1.13 \times 10^6$ m/s and $\epsilon_b \approx 5$.

Figure 2(a) shows such plots for some intraband and interband channels, using $v_0^{\rm ren}|_{B=10\ \mathrm{T}} \approx 1.13 \times 10^6$ m/s which fits the $0 \to 1$ resonance data, and, as a typical value, $V_c = \alpha/(\epsilon_b \ell) \approx 12\sqrt{B[\mathrm{T}]}$ meV ($\epsilon_b \sim 5$).

Actually, experiment[19] has already observed a small deviation of the $1:(1+\sqrt{2})$ ratio of $\epsilon_{\mathbf{k}=0}^{1\leftarrow 0}$ to $\epsilon_{\mathbf{k}=0}^{2\leftarrow -1}$ well outside of the experimental errors under high magnetic fields $B=(6-18)$ T; the data are apparently electron-hole symmetric, $\epsilon_{\mathbf{k}=0}^{1\leftarrow 0} \approx \epsilon_{\mathbf{k}=0}^{0\leftarrow -1}$. Figure 2(a) includes such data reproduced from Ref. 19. A small increase in $v_0^{\rm ren}$ in $\epsilon_{\mathbf{k}=0}^{2\leftarrow -1}/(\sqrt{2}+1)$, relative to $\epsilon_{\mathbf{k}=0}^{1\leftarrow 0}$, is roughly consistent with Eq. (3.20) which suggests a $0.122 V_c/\omega_c^{\rm ren} \sim 4\%$ increase in $v_0^{\rm ren}$ (since $V_c/\omega_c^{\rm ren} \sim 0.3$).

This feature is clearer from Fig. 2(b), which plots the $\epsilon_{\mathbf{k}=0}^{1\leftarrow 0}$ and $\epsilon_{\mathbf{k}=0}^{2\leftarrow -1}/(\sqrt{2}+1)$ data as a function of B in units of $\omega_c = \sqrt{2}v_0/\ell \propto \sqrt{B}$ (with $v_0 \to v_0^{\rm ren}|_{B=10\ \mathrm{T}}$). The deviation of the $(-1 \to 2)$ resonance data is more pronounced. In the figure a dotted curve represents a possible profile of the running of $v_0^{\rm ren}$ with B, and, especially, the $(-1 \to 2)$ data (with smaller error bars) suggests such running.

It is too early to draw any definite conclusion from the present data alone but the data is certainly consistent (in sign and magnitude) with the present estimate of the many-body effect. In this connection, let us note that an earlier experiment on thin epitaxial graphite[32] also observed the $(0 \to 1)$ and $(-1 \to 2)$ resonances with apparently no deviation from the $1:(1+\sqrt{2})$ ratio. This measurement was done under relatively weak magnetic fields $B=(0.4-4)$ T, and it could be that a small deviation, under larger error bars, simply escaped detection, apart from the potential difference between thin graphite and graphene.

More precise measurements of cyclotron resonance, especially in the high B domain where the Coulomb interaction becomes sizable, would be required to pin down the many-body effect in graphene. In this respect, the comparison between interband and intraband resonances from the *same* initial state, e.g., $-n \to \pm(n-1)$ at $\nu = 2-4n$ with $n=2,3,\ldots$, would provide a clearer signal for the many-body effect, with the influence of other possible sources reduced to a minimum. From Eqs. (3.18)–(3.21) one can read off the variations in $v_0^{\rm ren}$

$$\Delta R(-2 \to \pm 1) \overset{\nu=-6}{\approx} 0.34 V_c/\omega_c^{\rm ren} \sim 10\%,$$

$$\Delta R(-3 \to \pm 2) \overset{\nu=-10}{\approx} 0.40 V_c/\omega_c^{\rm ren} \sim 12\%, \qquad (3.22)$$

which imply that a comparison of the $(-2 \to \pm 1)$ resonances and that of the $(-3 \to \pm 2)$ resonances would find variations in v_0, about three times larger than the $\sim 4\%$ variation for $\epsilon_{\mathbf{k}=0}^{2\leftarrow -1}/(\sqrt{2}+1)$ vs $\epsilon_{\mathbf{k}=0}^{0\leftarrow -1}$ at $\nu=-2$.

IV. CYCLOTRON RESONANCES IN BILAYER GRAPHENE

In this section we consider cyclotron resonance in bilayer graphene. In bilayer graphene the electrons are described by four-component spinor fields on the four inequivalent sites (A,B) and (A',B') in the bottom and top layers, arranged in Bernal $A'B$ stacking. Interlayer coupling[33] $\gamma_1 \equiv \gamma_{A'B} \sim (0.3-0.4)$ eV modifies the intralayer linear spectra $\pm v_0|\mathbf{p}|$ to yield, in the low-energy branches $|\epsilon| < \gamma_1$, quasiparticles with a parabolic dispersion.[10] They, in a magnetic field, lead to a particle-hole symmetric tower of Landau levels $\{L_n\}$ ($n=0_\pm, \pm 1, \ldots$) with spectrum

$$\epsilon_n = s_n \omega_c \eta_n[(\gamma_1/\omega_c)^2], \qquad (4.1)$$

where $\eta_n(x) = \{(a_n + x - \sqrt{x^2 + 2a_n x + 1})/2\}^{1/2}$ with $a_n = 2|n| - 1$; see Appendix A The sequence of low-lying levels is made clearer in the form

$$\epsilon_n = s_n \omega^{\rm bi} \sqrt{|n|(|n|-1)}/\xi_n(w) \qquad (4.2)$$

with the characteristic cyclotron energy

$$\omega^{\rm bi} \equiv \omega_c^2/\gamma_1 = 2v_0^2/(\gamma_1 \ell^2) \sim 5B[\mathrm{T}]\ \mathrm{meV}, \qquad (4.3)$$

where $\xi_n(w) = \{(1 + a_n w + \sqrt{1 + 2a_n w + w^2})/2\}^{1/2}$ and $w \equiv (\omega_c/\gamma_1)^2 = \omega_c^{\rm bi}/\gamma_1 \sim 0.01B[\mathrm{T}] < 1$; $\xi_n(0) = 1$. The high-energy branches $|\epsilon| > \gamma_1$ of the spectra give rise to another tower of Landau levels with spectrum

$$\epsilon_n^+ = s_n \gamma_1 \xi_n(w), \qquad (4.4)$$

where $n = \pm 1, \pm 2, \ldots$.

Note that $\xi_n(w) = 1 + O(eB/\gamma_1)$. As a result, ϵ_n rises linearly with B at low energies $|\epsilon_n| < \gamma_1$ and turns into a $\sqrt{B}$ rise for $|\epsilon_n| \gg \gamma_1$. Both ϵ_n and ϵ_n^+ approach $\pm\sqrt{|n|}\omega_c$ for $|n| \to \infty$ since the bilayer turns into two isolated layers at short wavelengths.

In the bilayer there arise four zero-energy levels $\epsilon_n = 0$ with $n = (0_\pm, \pm 1)$ per spin. At one valley (say, K) they are electron levels with $n = (0_+, 1)$ and, at another valley, they are hole levels with $n = (0_-, -1)$; this feature is made explicit with a weak layer asymmetry, such as an interlayer voltage

which opens up a (tunable) band gap.[11–14] With a nonzero band gap, the zero-energy levels evolve into two quartets of nearly degenerate levels (separated by the gap), i.e., "pseudozero-mode" levels, which are expected to support pseudospin waves[34,35] as characteristic collective excitations.

For simplicity, we here turn off such a layer asymmetry as well as Zeeman splitting and the effect of trigonal warping (coming from $\gamma_3 \equiv \gamma_{AB'} < \gamma_1$). In view of the small layer separation, we do not distinguish between the intralayer and interlayer Coulomb interactions. Each Landau level L_n is thus treated as fourfold degenerate, except for the zero-mode levels (L_{0_+}, L_1) or (L_{0_-}, L_{-1}) which are fourfold degenerate at each valley.

The effective Hamiltonian for the electrons in bilayer graphene takes a 4×4 matrix form which, for studying the properties of the low-lying levels, may be reduced to an approximate 2×2 form.[10] Actually, the bending of the spectrum ϵ_n with B is appreciable in the high-B domain, $B=(10-20)$ T, where cyclotron resonance in bilayer graphene has been studied experimentally. Accordingly we employ the full four-component spinor description of the bilayer system; see Appendix A for details.

The charge density $\rho_{-\mathbf{p}}$ (for each spin and valley) takes the same form as Eq. (2.6) with $g^{kn}_{\mathbf{p}}$ replaced by

$$g^{kn}_{\mathbf{p}} = D_k D_n [f^{|k|,|n|}_{\mathbf{p}} + \beta^{(2)}_k \beta^{(2)}_n f^{|k|-2,|n|-2}_{\mathbf{p}} + (\beta^{(3)}_k \beta^{(3)}_n + \beta^{(4)}_k \beta^{(4)}_n) f^{|k|-1,|n|-1}_{\mathbf{p}}]; \tag{4.5}$$

see Appendix A for the coefficients $\{\beta^{(i)}_n\}$ and D_n. The sets $(\epsilon_n, g^{kn}_{\mathbf{p}})$ at the K and K' valleys are related as

$$\epsilon_n|_{K'} = -\epsilon_{-n}|_K, \quad g^{kn}_{\mathbf{p}}|_{K'} = g^{-k,-n}_{\mathbf{p}}|_K. \tag{4.6}$$

Actually, for zero band gap, $g^{kn}_{\mathbf{p}}$ are essentially the same at the two valleys since one further finds that

$$g^{kn}_{\mathbf{p}}|_{K'} = g^{kn}_{\mathbf{p}}|_K, \quad g^{k,-1}_{\mathbf{p}}|_{K'} = g^{k,1}_{\mathbf{p}}|_K, \quad g^{k,0_-}_{\mathbf{p}}|_{K'} = g^{k,0_+}_{\mathbf{p}}|_K \tag{4.7}$$

for $|k|\geq 2$ and $|n|\geq 2$.

One can now use the SMA formula (3.9) to calculate the interlevel excitation energies $\epsilon^{\rm exc}_{\mathbf{k}} = \epsilon_b - \epsilon_a + \Delta\epsilon^{b\leftarrow a}_{\mathbf{k}}$. The result applies to both valleys if one specifies the zero-mode levels accordingly. It is important to remember that for bilayer graphene the sum Σ_n over filled levels involves two branches ϵ_{-n} and ϵ^+_{-n} in the valence band.

Cyclotron resonance in bilayer graphene again obeys the selection rule[31] $\Delta|n| = \pm 1$; see Appendix B and Fig. 3(a). The Coulombic corrections $\Delta\epsilon^{b\leftarrow a}_{\mathbf{k}=0}$ are diagonal in spin and valley (while mixing arises for $\mathbf{k}\neq 0$). The vacuum-polarization effect again makes $\Delta\epsilon^{b\leftarrow a}_{\mathbf{k}=0}$ cutoff dependent.

For renormalization let us first look into the $B=0$ case. One can construct the electron propagator and, as in the monolayer case, calculate the Coulombic quantum corrections. It turns out that not only v_0 but also γ_1 undergo infinite renormalization and, rather unexpectedly, the divergent terms are the same for both of them to $O(V_c)$ at least; they also coincide with the divergent term in the monolayer case; see Appendix C for details. To be precise, the divergences are removed, to $O(V_c)$ of our present interest, by rescaling

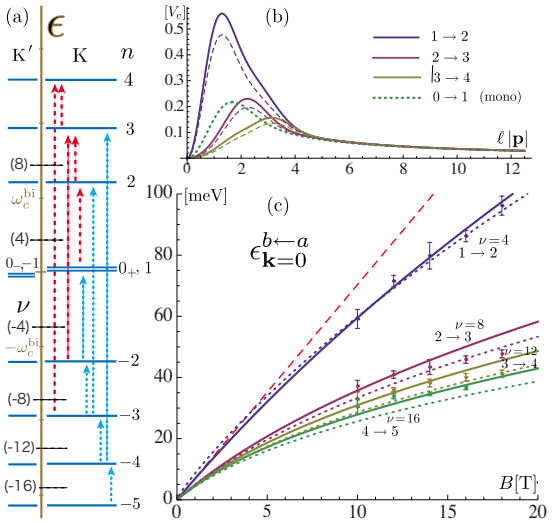

FIG. 3. (Color online) (a) Cyclotron resonance in bilayer graphene. (b) Momentum profiles of the bilayer many-body corrections $\Delta\epsilon^{n+1\leftarrow n}_{\mathbf{k}=0}/(\eta_{n+1}-\eta_n)$ for $n=1$, 2, and 3, with $\hat{v}_0=1.15$ and $\hat{\gamma}_1=3.5$; real curves at $B=10$ T and dashed curves at $B=16$ T. A dotted curve refers to the profile of the monolayer $(0\rightarrow 1)$ resonance. (c) Resonance energies as a function of B; real curves, with $\hat{v}_0=1.15$, $\hat{\gamma}_1=3.5$, and $V_c=0$; dotted curves, with $\hat{v}_0=1.15$, $\hat{\gamma}_1=3.8$, and $V_c\approx 5.6\sqrt{B[\mathrm{T}]}$ meV (or $\epsilon_b\approx 10$). The experimental data with error bars are reproduced from Ref. 21. Note that the low-lying $n=2$ spectrum ϵ_2 (equal to the $\nu=4$ curve) significantly deviates from the approximate spectrum $\epsilon_2\approx\sqrt{2}\omega^{\rm bi}_c$ with $\xi_2(w)\rightarrow 1$ (dashed line $\propto B$) for $B>10$ T.

$$v_0 = Z v_0^{\rm ren}, \quad \gamma_1 = Z\gamma_1^{\rm ren} \tag{4.8}$$

with a common factor Z.

This scaling tells us how to carry out renormalization in the presence of a magnetic field B. Let us write, as in Eq. (3.18) of the monolayer case, the excitation energy for the $L_n\rightarrow L_k$ transition in the form

$$\epsilon^{k\leftarrow n}_{\mathbf{k}=0} = (s_k\eta_k - s_n\eta_n)(\sqrt{2}v_0/\ell + c^{kn}V_c) \tag{4.9}$$

with $\eta_n=\eta_n(1/w)$. Note first that $v_0/\gamma_1 = v_0^{\rm ren}/\gamma_1^{\rm ren}$ is invariant under renormalization; it is therefore finite and does not run with B. Similarly, $w=(\omega_c/\gamma_1)^2\propto(v_0^{\rm ren}/\gamma_1^{\rm ren})^2 B$ is invariant and is linear in B. This means that $\eta_n(1/w)$ remain unrenormalized and finite. Equation (4.9) then reveals a remarkable structure of the Coulombic corrections c^{kn}: The divergent pieces are common to all c^{kn} and are removed by a single counterterm $\propto(Z-1)v_0^{\rm ren}$.

Figure 3(b) depicts the momentum profiles $\gamma^2_{\mathbf{p}}[\cdots]$ of $\Delta\epsilon^{k\leftarrow n}_{\mathbf{k}=0}/(s_k\eta_k - s_n\eta_n)$ for some typical resonances. For comparison the profile for the monolayer resonance $(\Delta\epsilon^{1\leftarrow 0}_{\mathbf{k}=0})^{\rm mono}$ is also included there. The gradually decreasing high-momentum tails, common to all, numerically demonstrate the validity of the scaling in Eqs. (4.8) and (4.9). This further verifies that the leading logarithmic velocity renormalization is formally the same for both monolayer and bilayer graphene.

For renormalization let us refer to a specific resonance, e.g., the $-3\to-2$ resonance at $\nu=-8$, and define $v_0^{\rm ren}$ so as to absorb its entire $O(V_c)$ correction

$$\omega_c^{\rm ren}\equiv\sqrt{2}v_0^{\rm ren}|_B/\ell=\sqrt{2}v_0/\ell+c^{-2,-3}V_c. \tag{4.10}$$

One then has, for general $n\to k$ channels

$$\epsilon_{\mathbf{k}=0}^{k\leftarrow n}=(s_k\eta_k-s_n\eta_n)(\omega_c^{\rm ren}+\Delta c^{kn}V_c). \tag{4.11}$$

Here $\Delta c^{kn}\equiv c^{kn}-c^{-2,-3}$ are now free from the UV divergence and are uniquely fixed as genuine quantum corrections. In terms of the bilayer cyclotron frequency $(\omega^{\rm bi})^{\rm ren}\equiv(\omega_c^{\rm ren})^2/\gamma_1^{\rm ren}$, this also reads

$$\epsilon_{\mathbf{k}=0}^{k\leftarrow n}=(s_k\zeta_k-s_n\zeta_n)\{(\omega^{\rm bi})^{\rm ren}+\Delta c^{kn}\sqrt{w}V_c\} \tag{4.12}$$

with $\zeta_n=\sqrt{|n|(|n|-1)}/\xi_n(w)$ and $w=(\omega^{\rm bi})^{\rm ren}/\gamma_1^{\rm ren}$.

The quantum corrections Δc^{kn}, unlike those of the monolayer case, are not pure numbers and, actually, are functions of $\sqrt{w}=\omega_c^{\rm ren}/\gamma_1^{\rm ren}$. This is seen if one notes that $g_{\mathbf{p}}^{kn}$ are functions of $\sqrt{w}$ and $\ell\mathbf{p}$ so that c^{kn} are functions of $\sqrt{w}$ and the cutoff $N_L\propto\Lambda^2/(eB)$; the cutoff-independent corrections Δc^{kn} thus depend on w alone. Let us set $\gamma_1^{\rm ren}=\hat{\gamma}_1\times100$ meV and $v_0^{\rm ren}=\hat{v}_0\times10^6$ m/s so that $1/\sqrt{w}=\gamma_1^{\rm ren}/\omega_c^{\rm ren}\approx2.75G$ with $G=\hat{\gamma}_1/(\hat{v}_0\sqrt{B[\mathrm{T}]})$; $G=1$ for $\hat{\gamma}_1=3.5$ and $\hat{v}_0\approx1.107$ at $B=10$ T. It turns out that $\Delta c^{k,n}$, when plotted in G, behave almost linearly around $G=1$.

The way $v_0^{\rm ren}$ runs with B is determined from

$$v_0^{\rm ren}|_B=v_0^{\rm ren}|_{B_0}+\delta c^{-2,-3}\alpha/(\sqrt{2}\epsilon_b), \tag{4.13}$$

where $\delta c^{-2,-3}\equiv c^{-2,-3}|_B-c^{-2,-3}|_{B_0}$. Numerically $\delta c^{-2,-3}$ is nearly twice as large as the monolayer expression $-(\sqrt{2}/8)\log(B/B_0)$ over the range $0.5<B/B_0<2$ around $G=1$. The decrease in $v_0^{\rm ren}|_B$ with B is larger in bilayer graphene and may amount to about 7% for $B/B_0\sim2$ (and $\epsilon_b\sim5$). In this way, the renormalized velocity $v_0^{\rm ren}$ is in general different, in magnitude and running with B, for monolayer and bilayer graphene; it reflects their low-energy features as well.

We are now ready to look into some typical channels of cyclotron resonance. We use Eq. (4.11) and evaluate $\Delta c^{k,n}\equiv\Delta c^{k\leftarrow n}$ numerically; for the bilayer the filling factor $\nu=4(n_{\rm f}+1)$ for $n_{\rm f}\le-2$ while $\nu=4n_{\rm f}$ for $n_{\rm f}\ge1$. For intraband channels one finds

$$\Delta c^{\pm1,-2}\overset{\nu=-4}{=}0.7270+0.5484\delta G,$$

$$\Delta c^{-2,-3}\overset{\nu=-8}{=}0,$$

$$\Delta c^{-3,-4}\overset{\nu=-12}{=}-0.1521-0.0453\delta G,$$

$$\Delta c^{-4,-5}\overset{\nu=-16}{=}-0.2496-0.0797\delta G, \tag{4.14}$$

where $\delta G=G-1$ with $G=\hat{\gamma}_1/(\hat{v}_0\sqrt{B[\mathrm{T}]})$. Similarly, for interband resonances one obtains

$$\Delta c^{3\leftarrow-2}\overset{\nu=-4}{=}0.3922-0.0023\delta G,$$

$$\Delta c^{2\leftarrow-3}\overset{\nu=-4}{=}0.4794+0.0706\delta G,$$

$$\Delta c^{2\leftarrow-3}\overset{\nu=-8}{=}0.3872+0.0552\delta G,$$

$$\Delta c^{3\leftarrow-4}\overset{\nu=-12}{=}0.2961+0.00145\delta G; \tag{4.15}$$

also $\Delta c^{4\leftarrow-3}\overset{\nu=-4}{=}0.41+\cdots$ and $\Delta c^{4\leftarrow-3}\overset{\nu=-8}{=}0.29+\cdots$. These linearized expressions are numerically precise with errors of less than 3% over the range $0.3<G<1.5$. The many-body effect is thus expected to be sizable in bilayer graphene. An effective variation in $v_0^{\rm ren}$ would amount to about $0.7V_c/\omega_c^{\rm ren}\sim20\%$ for $\epsilon_{\mathbf{k}=0}^{1\leftarrow-2}|_{\nu=-4}$ and about -5% for $\epsilon_{\mathbf{k}=0}^{-3\leftarrow-4}|_{\nu=-12}$, in comparison with $\epsilon_{\mathbf{k}=0}^{-2\leftarrow-3}|_{\nu=-8}$.

As for experiment, Henriksen *et al.*[21] measured, via IR spectroscopy, cyclotron resonance in bilayer graphene in magnetic fields up to 18 T. They observed intraband transitions, which are identified with $\{\epsilon_{\mathbf{k}=0}^{2\leftarrow1}|_{\nu=4},\epsilon_{\mathbf{k}=0}^{3\leftarrow2}|_{\nu=8},\epsilon_{\mathbf{k}=0}^{4\leftarrow3}|_{\nu=12},\epsilon_{\mathbf{k}=0}^{5\leftarrow4}|_{\nu=16}\}$ and the corresponding hole resonances listed in Eq. (4.14), together with an appreciable asymmetry between the electron and hole data.

Figure 3(c) reproduces the electron data of Ref. 21. There the real curves represent the resonance energies in Eq. (4.11) for $V_c=0$, with $\hat{v}_0\approx1.15$ deduced from the $\nu=4$ data and $\hat{\gamma}_1$ taken to be 3.5, as supposed in Ref. 21. They poorly fit the $\nu=8,12,16$ data. Unfortunately, inclusion of the $O(V_c)$ corrections scarcely improves the fit, as seen from the dotted curves.

The situation becomes clearer if one, in view of Eq. (4.11), reorganizes the experimental data in the form $\epsilon_{\mathbf{k}=0}^{k\leftarrow n}/(s_k\eta_k-s_n\eta_n)$ and plots them in units of $\omega_c=\sqrt{2}v_0/\ell$ (with $v_0=1.15\times10^6$ m/s). Figure 4(a) shows such a plot for the electron data; for clarity the data points for different channels, originally at $B=(10,12,14,16)$ T, are slightly shifted in B. It is to be contrasted with Fig. 4(b), which illustrates how each resonance would behave with B, according to Eq. (4.11), for $V_c\approx10\sqrt{B[\mathrm{T}]}$ meV (or $\epsilon_b\approx5.6$); in particular, the $\nu=8$ curve represents the running of $v_0^{\rm ren}|_B$ according to Eq. (4.13). In Fig. 4(a) the $\nu=8,12,16$ resonances are apparently ordered in a way opposite to Fig. 4(b), and an appreciable gap between the $\nu=4$ resonance and the rest is not very clear. The $\nu=8,12,16$ data show a general trend to decrease with B, consistent with possible running of $v_0^{\rm ren}|_B$ but at a rate faster than expected. It is rather difficult to interpret these features, but they, in part, could be attributed to possible quantum screening[35] of the Coulomb interaction in bilayer graphene such that ϵ_b is effectively larger[36] for lower B. Note, in this connection, Fig. 4(c) which shows that the same data may suggest a Coulombic gap for a choice $\gamma_1\approx4$ favored in Ref. 33. We further remark that, in spite of an asymmetry in electron and hole data, the hole data shares essentially the same features; see Fig. 4(d).

No data are available for interband cyclotron resonance in bilayer graphene at present. They are highly desired because the comparison of interband and intraband resonances from the same initial states would provide a clearer signal for the many-body effect. We record the ratios

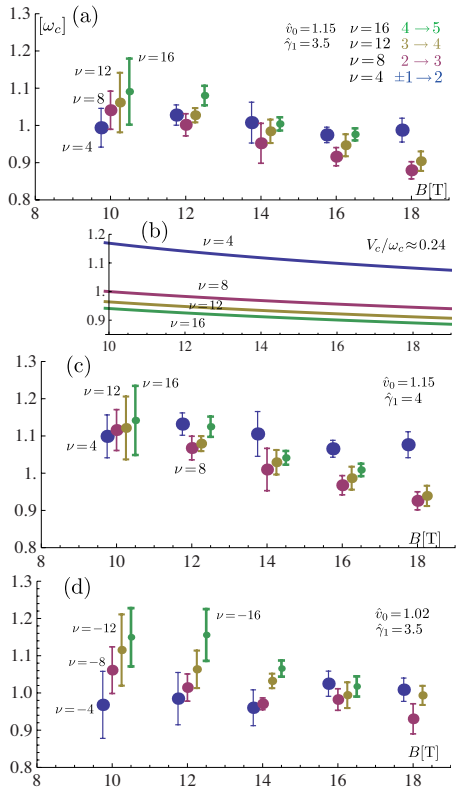

FIG. 4. (Color online) Experimental data of Ref. 21, reorganized in the form $\epsilon_{\mathbf{k}=0}^{k\leftarrow n}/(s_k\eta_k - s_n\eta_n)$ and plotted in units of $\omega_c=\sqrt{2}v_0/\ell^2$ (with $v_0=1.15\times10^6$ m/s). (a) Electron data, analyzed with $\hat{v}_0=1.15$ and $\hat{\gamma}_1=3.5$; for clarity the data points, originally at $B=(10,12,14,16)$ T, are slightly shifted in B. (b) Theoretical expectation according to Eq. (4.11) with $\hat{v}_0=1.14$, $\hat{\gamma}_1=3.5$, and $V_c/\omega_c\approx0.24$ (or $\epsilon_b\approx5.6$). (c) Electron data, reanalyzed with $\hat{\gamma}_1=4$. (d) Hole data, analyzed with $\hat{v}_0=1.02$ and $\hat{\gamma}_1=3.5$.

$$\Delta R(-3\to\pm2)\overset{\nu=-8}{\approx}0.39V_c/\omega_c^{\rm ren}\sim15\%,$$

$$\Delta R(-4\to\pm3)\overset{\nu=-12}{\approx}0.45V_c/\omega_c^{\rm ren}\sim18\%, \qquad (4.16)$$

which imply that a close look into the $(-3\to\pm2)$ resonances and the $(-4\to\pm3)$ resonances would find a sizable variation $\sim15\%$ in $v_0^{\rm ren}$.

V. SUMMARY AND DISCUSSION

Graphene supports charge carriers that behave as Dirac fermions, which, in a magnetic field, lead to a characteristic particle-hole symmetric pattern of Landau levels. Accordingly, unlike standard QH systems, there is a rich variety of cyclotron resonance, both intraband and interband resonances of various energies, in graphene.

In this paper we have studied many-body corrections to cyclotron resonance in graphene. We have constructed an effective theory using the SMA and noted that genuine nonzero many-body corrections (not due to fine splitting in spin or valley) derive from the quantum fluctuations of the vacuum (the Dirac sea). Such quantum corrections are intrinsically ultraviolet divergent and, as we have emphasized, it is necessary to carry out renormalization of velocity v_0 (and, for bilayer graphene, interlayer coupling γ_1 as well) to determine the many-body corrections uniquely in terms of physical quantities. As a result, the observable intralayer and interlayer coupling strengths $v_0^{\rm ren}\propto\gamma_0^{\rm ren}$ and $\gamma_1^{\rm ren}$ in general run with the magnetic field B.

Experimental data on cyclotron resonance generally have sizable error bars, which make a clear identification of the many-body effect difficult. In this respect, we have presented a way to analyze the data, as in Figs. 2(b) and 4, with the effect of renormalization properly taken into account.

For monolayer graphene a piece of data[19] which compares some leading interband and intraband resonances is apparently consistent with the presence of many-body corrections roughly in magnitude and sign, and also in the running of $v_0^{\rm ren}$ with B. For bilayer graphene the existing data are only for intraband resonances and are rather puzzling, as discussed in Sec. IV. They generally appear to defy good fit by theory but certainly suggest nontrivial features of many-body corrections, such as running with B.

More precise measurements of cyclotron resonances are highly desired. Of particular interest are experiments which compare interband and intraband resonances from the same initial states, as listed in Eqs. (3.22) and (4.16), which would clarify the many-body effect with minimal uncertainties.

ACKNOWLEDGMENTS

This work was supported in part by a Grant-in-Aid for Scientific Research from the Ministry of Education, Science, Sports and Culture of Japan (Grant No. 21540265).

APPENDIX A: LANDAU LEVELS IN BILAYER GRAPHENE

This appendix summarizes the effective Hamiltonian and its eigenfunctions for bilayer graphene in a magnetic field B. The bilayer Hamiltonian with interlayer coupling $\gamma_1\equiv\gamma_{A'B}$ is written, at one (K) valley, as[10]

$$H^{\rm bi}=\begin{pmatrix}0 & & & v_0\Pi^\dagger\\ & 0 & v_0\Pi & \\ & v_0\Pi^\dagger & 0 & \gamma_1\\ v_0\Pi & & \gamma_1 & 0\end{pmatrix}, \qquad (A1)$$

which acts on an electron field of the form $\Psi_K=(\psi_A,\psi_{B'},\psi_{A'},\psi_B)^t$ in obvious notation; $\Pi=\Pi_x-i\Pi_y$ and $\Pi^\dagger=\Pi_x+i\Pi_y$ with $A_i\to B(-y,0)$.

The energy eigenvalues obey the equation

$$(|n|-1-\epsilon'^2)(|n|-\epsilon'^2)-\gamma'^2(\epsilon')^2=0, \qquad (A2)$$

where $\epsilon'\equiv\epsilon_n/\omega_c$, $\gamma'\equiv\gamma_1/\omega_c$, and $\omega_c=\sqrt{2}v_0/\ell$. This leads to the two branches of spectra $(\epsilon_n,\epsilon_n^+)$ in Eqs. (4.1) and (4.4). In particular, zero energy $\epsilon_n=0$ is possible for $|n|=0$ or $|n|=1$ while $|\epsilon_{\pm1}^+|>\gamma_1$. A weak interlayer voltage $\frac{1}{2}(\delta V)\mathrm{diag}[1,-1,-1,1]$, added to $H^{\rm bi}$, reveals that the zero modes actually have $n=0_+$ and $n=1$ for $\delta V>0$.

The corresponding eigenfunctions for $n=\pm2,\pm3,\ldots$ take the form

$$\Psi_n = D_n \begin{pmatrix} ||n|\rangle \\ \beta_n^{(2)}||n|-2\rangle \\ \beta_n^{(3)}||n|-1\rangle \\ \beta_n^{(4)}||n|-1\rangle \end{pmatrix},$$

$$\beta_n^{(2)} = \frac{\sqrt{|n|-1}}{\epsilon'}\beta_n^{(3)}, \quad \beta_n^{(3)} = -\frac{1}{\gamma'}\frac{|n|-\epsilon'^2}{\sqrt{|n|}}, \tag{A3}$$

$$\beta_n^{(4)} = \frac{\epsilon'}{\sqrt{|n|}}, \quad D_n = \frac{1}{\sqrt{2}}\sqrt{\frac{|n|(|n|-1-\epsilon'^2)}{|n|(|n|-1)-\epsilon'^4}}, \tag{A4}$$

where only the orbital eigenmodes are shown using the standard harmonic-oscillator basis $\{|n\rangle\}$. These expressions for Ψ_n are equally valid for both the low- and high-energy branches ϵ_n and ϵ_n^+ of Landau levels, depending on ϵ' one employs.

The zero-energy eigenmodes are given by

$$\Psi_{0_+} = (|0\rangle, 0, 0, 0)^t,$$

$$\Psi_1 = D_1(|1\rangle, 0, -(1/\gamma')|0\rangle, 0)^t, \tag{A5}$$

with $D_1 = (1+1/\gamma'^2)^{-1/2}$.

At another (K') valley the Hamiltonian is given by Eq. (A1) with $v_0 \to -v_0$ and acts on a field of the form $\Psi_{K'} = (\psi_{B'}, \psi_A, \psi_B, \psi_{A'})^t$. Accordingly one finds that

$$\epsilon_n|_{K'} = -\epsilon_{-n}|_K, \quad D_n|_{K'} = D_{-n}|_K, \quad \beta_n^{(2)}|_{K'} = \beta_{-n}^{(2)}|_K,$$

$$\beta_n^{(3)}|_{K'} = -\beta_{-n}^{(3)}|_K, \quad \beta_n^{(4)}|_{K'} = -\beta_{-n}^{(4)}|_K. \tag{A6}$$

The zero-energy levels now have $n=0_-$ and $n=-1$.

APPENDIX B: COUPLING TO CURRENT

Consider a weak time-varying vector potential $[A_x(t), A_y(t)]$ coupled to the total current in graphene. For the effective Lagrangian L_Φ in Eq. (3.4) this yields coupling of A_i to $\Phi^{kn}_{\mathbf{k}=0} = \int d^2\mathbf{x}\Phi^{kn}$ of the form

$$H_A = -i\frac{e\ell\omega_c}{\sqrt{2}}\sqrt{\rho_0}d_n\{A\Phi^{\pm(n-1),-n}_{\mathbf{k}=0} + A^\dagger\Phi^{n,\pm(n-1)}_{\mathbf{k}=0}\} + \text{H.c.}, \tag{B1}$$

where $d_n = \pm 1/2$ for $n \geq 2$ and $d_1 = \pm 1/\sqrt{2}$; $A = A_x - iA_y$; and $\rho_0 = 1/(2\pi\ell^2)$. The cyclotron resonance thus obeys the selection rule $\Delta|n| = \pm 1$. In particular, the $-n \to \pm(n-1)$ transitions and the $\pm(n-1) \to n$ transitions ($n \geq 1$) are distinguished[31] by use of circularly polarized light $\propto A_x \pm iA_y$.

Equation (B1) (with $n \geq 2$) applies to the case of bilayer graphene as well if one sets $\omega_c \to \omega_c^{\text{bi}}$, $A^\dagger \to -A^\dagger$, $d_n = \sqrt{n-1}$ for $n \geq 3$, and $d_2 = \sqrt{2}$, apart from terms of $O[(\omega_c/\gamma_1)^2]$.

APPENDIX C: PROPAGATORS

In this appendix we derive the electron propagator for bilayer graphene in free space. Let us set $\Pi \to p_x - ip_y$ in H^{bi} of Eq. (A1) and consider the propagator

$$\langle\Psi(x)\Psi^\dagger(x')\rangle = \langle x|1/(i\partial_t - H^{\text{bi}})|x'\rangle \tag{C1}$$

with $|x\rangle \equiv |\mathbf{x}\rangle|t\rangle$. We divide the 4×4 matrix H^{bi} into a 2×2 block form and invert $(i\partial_t - H^{\text{bi}})$. In Fourier $(\mathbf{p}, \omega)$ space the propagator reads, in 2×2 block form

$$\langle\Psi\Psi^\dagger\rangle_{11} = \frac{i}{D}\{\omega(\omega^2 - v_0^2\mathbf{p}^2 - \gamma_1^2) + \gamma_1 v_0^2 P\sigma_1 P\},$$

$$\langle\Psi\Psi^\dagger\rangle_{21} = \frac{i}{D}(\omega^2 - v_0^2\mathbf{p}^2 + \omega\gamma_1\sigma_1)v_0 P,$$

$$\langle\Psi\Psi^\dagger\rangle_{12} = \frac{i}{D}v_0 P(\omega^2 - v_0^2\mathbf{p}^2 + \omega\gamma_1\sigma_1),$$

$$\langle\Psi\Psi^\dagger\rangle_{22} = i\frac{\omega}{D}(\omega^2 - v_0^2\mathbf{p}^2 + \omega\gamma_1\sigma_1), \tag{C2}$$

where $D = (v_0^2\mathbf{p}^2 - \omega^2)^2 - \omega^2\gamma_1^2 = (\omega^2 - E_+^2)(\omega^2 - E_-^2)$ with $E_\pm = \sqrt{\gamma_1^2/4 + v_0^2\mathbf{p}^2} \pm \gamma_1/2$; $P = p^\dagger\sigma_+ + p\sigma_-$ and $P\sigma_1 P = (p^\dagger)^2\sigma_+ + p^2\sigma_-$ with $p = p_x - ip_y$, $p^\dagger = p_x + ip_y$, and $\sigma_\pm = (\sigma_1 \pm i\sigma_2)/2$.

This leads to the instantaneous propagator $\int(d\omega/2\pi)\langle\Psi\Psi^\dagger\rangle$, giving

$$\langle\Psi\Psi^\dagger\rangle|_{t=t'} = \frac{1}{4\mathcal{D}_\mathbf{p}}\begin{pmatrix} \gamma_1 P\sigma_1 P/\mathbf{p}^2 & 2v_0 P \\ 2v_0 P & \gamma_1\sigma_1 \end{pmatrix} \tag{C3}$$

with $\mathcal{D}_\mathbf{p} = \sqrt{\gamma_1^2/4 + v_0^2\mathbf{p}^2}$.

To calculate the Coulomb exchange correction one may replace, in Eq. (3.13), $iS(\mathbf{p})$ by this propagator. Note that $v_0 P/(2\mathcal{D}_\mathbf{p})$ approaches, for $\mathbf{p} \to \infty$, the monolayer propagator $iS(\mathbf{p}) = \sigma_i p_i/(2|\mathbf{p}|)$ (apart from an inessential mismatch $\sigma_2 \to -\sigma_2$ in notation). As a result, setting $iS(\mathbf{p}) \to v_0 P/(2\mathcal{D}_\mathbf{p})$ for v_0 and $iS(\mathbf{p}) \to \gamma_1/(4\mathcal{D}_\mathbf{p})$ for γ_1 and carrying out the $\mathbf{k}$ integration, as in Eq. (3.13), yield the same amount of logarithmic divergence $\sim(\alpha/8\epsilon_b)\log\Lambda^2$ as in the monolayer case; it thus renormalizes v_0 and γ_1 simultaneously as in Eq. (4.8).

[1] K. S. Novoselov, A. K. Geim, S. V. Morozov, D. Jiang, M. I. Katsnelson, I. V. Grigorieva, S. V. Dubonos, and A. A. Firsov, Nature (London) **438**, 197 (2005).

[2] Y. Zhang, Y.-W. Tan, H. L. Stormer, and P. Kim, Nature (London) **438**, 201 (2005).

[3] Y. Zhang, Z. Jiang, J. P. Small, M. S. Purewal, Y.-W. Tan, M. Fazlollahi, J. D. Chudow, J. A. Jaszczak, H. L. Stormer, and P. Kim, Phys. Rev. Lett. **96**, 136806 (2006).

[4] N. H. Shon and T. Ando, J. Phys. Soc. Jpn. **67**, 2421 (1998); Y. Zheng and T. Ando, Phys. Rev. B **65**, 245420 (2002).
[5] V. P. Gusynin and S. G. Sharapov, Phys. Rev. Lett. **95**, 146801 (2005).
[6] N. M. R. Peres, F. Guinea, and A. H. Castro Neto, Phys. Rev. B **73**, 125411 (2006).
[7] G. W. Semenoff, Phys. Rev. Lett. **53**, 2449 (1984).
[8] A. J. Niemi and G. W. Semenoff, Phys. Rev. Lett. **51**, 2077 (1983).
[9] K. S. Novoselov, E. McCann, S. V. Morozov, V. I. Fal'ko, M. I. Katsnelson, U. Zeitler, D. Jiang, F. Schedin, and A. K. Geim, Nat. Phys. **2**, 177 (2006).
[10] E. McCann and V. I. Fal'ko, Phys. Rev. Lett. **96**, 086805 (2006).
[11] T. Ohta, A. Bostwick, T. Seyller, K. Horn, and E. Rotenberg, Science **313**, 951 (2006).
[12] E. McCann, Phys. Rev. B **74**, 161403(R) (2006).
[13] E. V. Castro, K. S. Novoselov, S. V. Morozov, N. M. R. Peres, J. M. B. Lopes dos Santos, J. Nilsson, F. Guinea, A. K. Geim, and A. H. Castro Neto, Phys. Rev. Lett. **99**, 216802 (2007).
[14] J. B. Oostinga, H. B. Heersche, X. Liu, A. F. Morpurgo, and L. M. K. Vandersypen, Nature Mater. **7**, 151 (2008).
[15] W. Kohn, Phys. Rev. **123**, 1242 (1961).
[16] For many-body corrections to two-component cyclotron resonance in QH systems see, K. Asano and T. Ando, Phys. Rev. B **58**, 1485 (1998).
[17] A. Iyengar, J. Wang, H. A. Fertig, and L. Brey, Phys. Rev. B **75**, 125430 (2007).
[18] Yu. A. Bychkov and G. Martinez, Phys. Rev. B **77**, 125417 (2008).
[19] Z. Jiang, E. A. Henriksen, L. C. Tung, Y.-J. Wang, M. E. Schwartz, M. Y. Han, P. Kim, and H. L. Stormer, Phys. Rev. Lett. **98**, 197403 (2007).
[20] R. S. Deacon, K.-C. Chuang, R. J. Nicholas, K. S. Novoselov, and A. K. Geim, Phys. Rev. B **76**, 081406(R) (2007).
[21] E. A. Henriksen, Z. Jiang, L.-C. Tung, M. E. Schwartz, M. Takita, Y.-J. Wang, P. Kim, and H. L. Stormer, Phys. Rev. Lett. **100**, 087403 (2008);See also E. A. Henriksen, P. Cadden-Zimansky, Z. Jiang, Z. Q. Li, L.-C. Tung, M. E. Schwartz, M. Takita, Y.-J. Wang, P. Kim, and H. L. Stormer, e-print id arXiv:0910.4575 (unpublished).
[22] The need for velocity and mass renormalization for electrons in bilayer graphene was earlier discussed in Ref. 23 with a phenomenological fit to the quasiparticle dispersion within the Thomas-Fermi approximation and Hartree-Fock theory.
[23] S. Viola Kusminskiy, D. K. Campbell, and A. H. Castro Neto, Euro. Phys. Lett. **85**, 58005 (2009).
[24] K. Shizuya, Phys. Rev. B **75**, 245417 (2007); **77**, 075419 (2008).
[25] S. M. Girvin, A. H. MacDonald, and P. M. Platzman, Phys. Rev. B **33**, 2481 (1986).
[26] K. Shizuya, Int. J. Mod. Phys. B **17**, 5875 (2003).
[27] K. Moon, H. Mori, K. Yang, S. M. Girvin, A. H. MacDonald, L. Zheng, D. Yoshioka, and S.-C. Zhang, Phys. Rev. B **51**, 5138 (1995).
[28] A. H. MacDonald and S. C. Zhang, Phys. Rev. B **49**, 17208 (1994).
[29] Here $\mathcal{C}_N=(\sqrt{2}/8)\Sigma_{k=1}^{N_L}\Gamma(k-1/2)\sqrt{k}/k!$, which is related to the quantities a in Ref. 17 and C_1 in Ref. 18 as $\mathcal{C}_N=a/V_c-(3/4)\sqrt{\pi/2}=C_1-(3/8)\sqrt{\pi/2}$.
[30] J. González, F. Guinea, and M.A.H. Vozmediano, Nucl. Phys. B **424**, 595 (1994).
[31] D. S. L. Abergel and V. I. Fal'ko, Phys. Rev. B **75**, 155430 (2007).
[32] M. L. Sadowski, G. Martinez, M. Potemski, C. Berger, and W. A. de Heer, Phys. Rev. Lett. **97**, 266405 (2006).
[33] L. M. Zhang, Z. Q. Li, D. N. Basov, M. M. Fogler, Z. Hao, and M. C. Martin, Phys. Rev. B **78**, 235408 (2008).
[34] Y. Barlas, R. Côté, K. Nomura, and A. H. MacDonald, Phys. Rev. Lett. **101**, 097601 (2008).
[35] K. Shizuya, Phys. Rev. B **79**, 165402 (2009); T. Misumi and K. Shizuya, *ibid.* **77**, 195423 (2008).
[36] An estimate in Ref. 24 gives $\epsilon_b|_{B=10\ \mathrm{T}}/\epsilon_b|_{B=20\ \mathrm{T}}\sim 1.3$.